Journal Pre-proof

The use of anion exchange pigments to inhibit the filiform corrosion of zinc-aluminium-magnesium coated steel

N. Wint, D. Eaves, G. Williams, H.N. McMurray

PII: S0010-938X(21)00652-1

DOI: https://doi.org/10.1016/j.corsci.2021.109886

Reference: CS109886

To appear in: *Corrosion Science*

Received date: 29 June 2021
Revised date: 1 October 2021
Accepted date: 11 October 2021

Please cite this article as: N. Wint, D. Eaves, G. Williams and H.N. McMurray, The use of anion exchange pigments to inhibit the filiform corrosion of zinc-aluminium-magnesium coated steel, *Corrosion Science,* (2021) doi:https://doi.org/10.1016/j.corsci.2021.109886

The use of anion exchange pigments to inhibit the filiform corrosion of zinc-aluminium-magnesium coated steel

N. Wint [a,*], D. Eaves [a], G. Williams [a], H. N. McMurray [a].

[a] *The Faculty of Science and Engineering, Swansea University, Bay Campus, Fabian Way, Crymlyn Burrow, Swansea, UK, SA1 8EN*

Abstract:

In-coating natural (carbonate exchanged) hydrotalcite is shown to significantly reduce the extent of filiform corrosion (FFC) on Zinc-Aluminium-Magnesium (ZAM) coated steels. The hydrotalcite pigment is dispersed within the model poly vinyl butyral (PVB) coating, which is then applied to ZAM. Acetic acid is applied to an artificial scribe penetrative PVB coating defect to initiate corrosion. Filiform corroded area and filament length are shown to decrease with increase in pigment volume fraction (ϕ). Tapering of filaments is also observed. Findings are consistent with hydrotalcite acting to sequester anions or neutralise the filiform head electrolyte.

Keywords; A Steel A Magnesium A Metal Coatings A Organic Coatings C Atmospheric Corrosion C Polymer Coatings.

*Corresponding author:
E-mail address: n.wint@swansea.ac.uk

1. Introduction

Coatings based on Zinc-aluminium-magnesium (ZAM) alloys are increasingly being used to afford cathodic protection to steel typically used within automotive and construction industries, with the aim of decreasing corrosion compared to more traditionally used Zn coatings. [1] ZAM coatings are typically overcoated with organic coatings to provide

further protection and allow for control of aesthetics. However, such layers are susceptible to failure, often via the formation of defects that penetrate the coating, allowing aggressive ions from an electrolyte to travel to the underlying metal [2]. In this paper we focus on the use of in-coating natural (carbonate exchanged) hydrotalcite (HT) to prevent a type of driven coating failure atmospheric corrosion, namely filiform corrosion (FFC), which can be initiated on ZAM by acetic acid, CH_3COOH (referred to throughout this paper as HAc) [3]. This research is timely and novel given both the lack of information pertaining to the inhibition of FFC as it occurs on industrially important ZAM coatings, and given increasing levels of legislation which bring an end to the use of traditionally used corrosion inhibitors.

FFC is a well-established form of localized corrosion which occurs at high relative humidity (60-95 % RH) [4-5] when an electrolyte breaches an organic coating and comes into contact with the metal underneath, resulting in anodic undercutting and subsequent detachment of the coating at the electrolyte containing filament 'head' [2, 4-6]. In the case of HAc induced FFC on ZAM, it is the intermetallic $MgZn_2$ which undergoes anodic dissolution at the head of the propagating filament [3]. The dissolution of the coating allows O_2 to percolate to the Fe substrate beneath, on which it takes part in the cathodic ORR, primarily at the back of the head. This differential aeration mechanism allows for the propagation of FFC [4-9], which takes the form of threads/ tracks of insoluble hydr(oxide) based corrosion product which precipitates under the organic coating in the path of the advancing head [4-5].

Although FFC can be initiated using $FeCl_2$, NaCl and HCl on iron [7-8, 10], aluminium [9, 11-17], and magnesium [18], only HAc, which is formed during numerous technological and biological processes [19-27], has been shown initiate FFC on ZAM reproducibly [3].

Efforts to prevent types of organic coating failure such as FFC have primarily been focused on the use of pigments based on hexavalent chromium (CrVI). However, the Cr(VI) compounds, which can be incorporated within a pre-treatment layer or as a pigment within a primer layer, are both carcinogenic and toxic [28-30] and alternative systems are a topic of current research. However, as of yet, there has not been any work pertaining to the inhibition of FFC as it occurs on ZAM.

One system which holds potential as an alternative corrosion inhibitor is hydrotalcite (HT), which takes the form of a white anionic clay. It is commercially available and consists of a layered structure of lamellar mixed hydroxides (both natural or synthetic), containing exchangeable anions [31]. It falls within the category of layered double hydroxides (LDH) which can exist in a wide variety of forms with different chemical compositions or crystallographic properties [32]. Equation 1 shows the general formula of this anionic clay where M^{2+} and M^{3+} are divalent and trivalent metal ions respectively, A^{n-} is the interlayer exchangeable anion and x has valences between ~ 0.25 and 0.33 [33].

$$[M^{2+}_{1-x}M^{3+}_{x}(OH)_2]^{x+}\,[A^{n-}_{\frac{x}{n}}yH_2O] \quad (1)$$

In this work we make use of a low-cost Mg/Al hydroxycarbonate $Mg_6Al_2(OH)_{16}(CO_3.4H_2O)$. The layered structure resembles that of brucite ($Mg[OH]_2$). However, the Al^{3+}ions, present within octahedral positions, are randomly substituted for Mg^{2+} ions, this resulting in the layer exhibiting a net positive charge. Electroneutrality is then maintained by exchangeable anions (typically CO_3^{2-}) which locate themselves in spaces between layers. Although a variety of anions can be incorporated [34-35], in nature, carbonate (CO_3^{2-}) anions fill the interlayer of HT [32, 36-37]. This property means that HT can be used in a variety of applications: in polymer systems as scavengers

of halogen; as halide getters in aqueous solutions [31, 33]; and to neutralize aqueous acid [31]. One notable example is within the PVC industry, where it acts as a scavenger of HCl [31] and as a medical antacid [38]. Other work has demonstrated the ability of HT to remove carboxylic acids including acetic acid from aqueous solution [39, 40]. This property also means that HTs are able to behave as exchangers (e.g. the interlayer anions can exchange with anions in an external media) that supply a wide range of anions which exchange with aggressive anions present within the filament head electrolyte [35]. This provides active corrosion inhibition whereby a stimuli (in this case the contact of an electrolyte) causes the release of anions from the organic coating matrix. This controlled release helps to prevent leaching, incomplete inhibition and osmotic blistering [41-42].

HT has been shown to inhibit FFC previously. For example, the inhibition of HCl induced FFC on AA2024 was attributed to the removal of Cl^- ions within the head electrolyte, as well as the progressive neutralization of the head electrolyte that occurred as the filaments came into contact with fresh in-coating HT [35]. A reaction between the metal and anions (released into the electrolyte during exchange) was also believed to result in chemical inhibition [35]. Other work has demonstrated the ability of HT to act as an exchange compound which can release zinc and vanadate ions to inhibitor corrosion of AA2024 [43-44]. More recently, LDH have been shown to inhibit FFC of AA5005 [45]. HT has also been used within a coating to prevent FFC of packaging material used in the presence of acids [46].

The present paper investigates the use of HT as a pigment which can be incorporated into organic coatings to inhibit FFC on ZAM. In so doing, varying amounts of HT pigment are dispersed within a model poly vinyl butyral (PVB) coating which is then applied to

ZAM samples. FFC is initiated using HAc, and FFC corroded area and filament length are recorded for each pigment volume fraction ($ø_{HT}$).

2. Materials and Methods

2.1 Materials

Production line material was obtained from Tata Steel Europe and consisted of 0.7 mm gauge mild steel with a 10 µm thick (140 $g.m^{-2}$) Zn-1.5 wt. % Al- 1.5 wt. % Mg coating layer on each side. 5 cm × 5 cm sized coupons were cut from the sheets and were cleaned using an aqueous slurry of 5 µm polishing alumina. They were then rinsed with distilled water and degreased in hexane before being left to air dry. Synthetic hydrotalcite (HT) and polyvinyl butyral-*co*-vinyl alcohol-*co*-vinyl acetate (PVB), molecular weight 70,000-100,000, as well as all the solvents and reagents used were supplied by the Sigma-Aldrich Chemical Company and of analytical grade.

2.2 Methods

Coating formulation; Synthetic pigment grade HT (1-5 µm particle size) was used as supplied, and therefore contained CO_3^{2-} anions and the dispersing agent stearic acid (octadecanoic acid) which acted as a dispersing agent. The anion- exchange capacity of HT was taken to be similar to that obtained in previous work which had made use of exhaustive back-exchange (using 0.1 M aqueous $Na2CO_3$) to calculate the quantity of exchangeable Cr_4^{2-} present in the $HT - Cr_4^{2-}$ pigment. The back-exchange solutions were analysed using ultraviolet-visible spectrophotometric analysis. 0.35 mmol of exchangeable Cr_4^{2-} was detected per gram of pigment, this corresponding to an anion-

exchange capacity of 0.7 milliequivalents (meq) g^{-1}. This is consistent with previously findings [33], but less than ca. 3 meq g^{-1}, the maximum value predicted for HT like compounds, when x in the general formula is ca. 0.3. HT pigments were dispersed into the PVB coating at four different pigment volume fractions ($ø_{HT}$). Whilst it is recognized that PVB is not representative of typical industrial coating systems, it was deemed a suitable coating for use in this work as it delaminates within a short time scale and therefore allows for a relatively efficient means of comparing the ability of a pigment to inhibit coating disbondment when incorporated within an organic coating. Equation 2, where M_{pol} is the mass of the polymer (0.8 $g.cm^{-3}$), ρ_{HT} is the density of the relevant pigment (2.06 $g.cm^{-3}$ for HT) and ρ_{pol} is the density of the polymer (1.083 $g.cm^{-3}$), can be used to calculate the HT pigment mass (M_{HT}) required for each value of $ø_{HT}$.

$$M_{HT} = \frac{\emptyset_{HT} \times M_{pol} \times \rho_{HT}}{(1-\emptyset_{HT}) \times \rho_{pol}} \quad (2)$$

The relevant amount of HT was dispersed within a small amount of ethanol to form an ethanolic slurry. This process aided the subsequent dispersion of HT within the relevant amount of 15.5 % w/w PVB and helped prevent HT agglomeration. The mixture was stirred thoroughly using a high shear mixer and maintained as a dispersion until used by more gentle agitation using a magnetic stirrer.

Materials Characterisation; A Hitachi TM3000 SEM was used to obtained images of filaments formed on ZAM. Prior to imaging, samples were ultra-sonicated in a hexane for 10 minutes to mechanically remove the PVB organic, and any corrosion product through cavitation.

Filiform Corrosion; Once the coupons had been cleaned and degreased, insulating tape was applied in strips onto two of the parallel edges and behaved as a height guide. A bar-casting process was used to apply PVB which was left dry, resulting in a thickness of 30 µm. A scalpel was used to produce 10 mm linear defects which penetrated the PVB. 2 µL aliquots of 1.5 mol.dm^{-3} HAc (pH~2) were applied to each defect using a micro syringe. Reservoirs of saturated $Na_2SO_410H_2O$ [2-3, 7-8, 13-15] were used to maintain a relative humidity (RH) of 93 % within an experimental chamber, into which the coupons were placed. Images of the sample surface were obtained on a weekly basis. Sample removal allowed for the chamber air to be refreshed. A Canon EOS was used to obtain images and measurements of FFC corroded area and filament length were taken using Sigma Scan Pro 5 software. The pre-measured real distance between two points in the image was used to calibrate the software. Corroded area was recorded for each scribe (2 per sample), resulting in four measurements for each $ø_{HT}$.

3. Results

3.1 Filiform Corrosion Study

The effect of in-coating HT $ø_{HT}$ on FFC inhibition was systematically studied following a methodology described previously whereby 2µL of 1.5 mol.dm^{-3} HAc was injected into the scribe defects [18]. Figure 1 shows optical images (representative) of PVB coated ZAM samples taken 1, 3 and 5 weeks after initiation. In the case of unpigmented PVB, FFC is observed within one week of initiation (Figure 1) and after 3 weeks, filaments have extended out and propagate away from the scribe in a perpendicular direction. Images were obtained for each $ø_{HT}$, and those acquired for 0.1 $ø_{HT}$ and 0.2 $ø_{HT}$ are shown in Figure 1. In both cases there is a delay in the initiation of FFC and there is very little

visible corrosion after 1 week. For coatings that contain 0.1 $ø_{HT}$, a small number of filaments are observed after 3 weeks. For 0.2 $ø_{HT}$, filaments are not clearly visible until 5 weeks after initiation. Images of the PVB coated ZAM samples after 5 weeks are shown in Figure 2. It is clear, from both the images and Table 1, that there are significantly less filaments present in the case of higher $ø_{HT}$. Filaments seem to take longer to become clearly established and are typically smaller in length.

(Figure 1)

(Figure 2)

(Table 1)

Total corroded area was obtained by digital image analysis of each type of sample. The values were obtained as a function of time for various $ø_{HT}$ and are plotted in Figure 3 and shown in Table 2. The confidence intervals correspond to ± one standard deviation on the mean of four measurements. The figure inset shows a portion of the graph at higher resolution which allows for a more detailed interrogation into the nature of the FFC kinetics. As can be seen, linear kinetics are observed for both the control and 0.05 $ø_{HT}$. In comparison, above 0.05 $ø_{HT}$, the growth of FFC corroded area tends to lower rates at longer holding times, as well as deviating from linearity.

For comparative purposes, the *initial* mean corroded area rate was assumed to be linear in all cases (independent of $ø_{HT}$) as it is deemed likely that 1.) the change in volume of the head electrolyte would be limited and 2.) the filament length is too small to allow cation migration to become rate determining within this short initial time period. The mean corroded area rate for each $ø_{HT}$ was obtained using linear regression (solid lines) and the values obtained are shown in Table 3. A rate of 0.23±0.01 $mm^2.week^{-1}$ was obtained for

$0ø_{HT}$, 0.11±0.01 $mm^2.week^{-1}$ for 0.05 $ø_{HT}$, 0.08±0.01 $mm^2.week^1$ for 0.10 $ø_{HT}$, and 0.05±0.01 $mm^2.week^{-1}$ for 0.15 $ø_{HT}$ and 0.01±0.01 $mm^2.week^{-1}$ for 0.20 $ø_{HT}$.

At this point, it should be borne in mind that it becomes increasingly difficult to determine the order of kinetics from an integrated rate plot in the case that FFC corroded area becomes small (as is true at higher $ø_{HT}$). Any claim regarding the linearity of FFC area-time plots must thus be caveated when inhibition or corrosion resistance makes the extent of area increase small over the experimental time period.

(Figure 3)

(Table 2)

(Table 3)

Filament length was obtained following a similar methodology as that used to obtain FFC corroded area. Figure 4 shows filament length as a function of time for various $ø_{HT}$. As can be seen, linear kinetics are observed for both the control and 0.05 $ø_{HT}$. However, above 0.05 $ø_{HT}$, the linear growth of FFC tends to lower rates at longer holding times.

The linear growth rate of FFC on samples coated in HT containing are worked out initially, and then after some time, to show that propagation slows at the higher $ø_{HT}$ (two phases represented by the solid and broken lines in Figure 4). The mean linear growth rate for each $ø_{HT}$ was obtained using linear regression (solid lines) and are shown in Table 3. A rate of 1.18±0.03 $mm.week^{-1}$ was obtained for $0ø_{HT}$, 0.79±0.02 $mm.week^{-1}$ (solid line) and 0.50±0.01 $mm.week^{-1}$ (broken line) for 0.05 $ø_{HT}$, 0.66±0.02 $mm.week^{-1}$ (solid line) and 0.59±0.09 $mm.week^{-1}$ (broken line) for 0.10 $ø_{HT}$, and 0.41±0.05 $mm.week^{-1}$ (solid line) and 0.46±0.01 $mm.week^{-1}$ (broken line) for 0.15 $ø_{HT}$ and 0.43±0.02 $mm.week^{-}$

[1] (solid line) and 0.28±0.02 mm.week^{-1} (broken line) for 0.20 $ø_{HT}$.

(Figure 4)

Figure 5 shows SEM images of filaments propagating on 1.5Al-1.5Mg coated steel for which the PVB overcoat contains a.) 0 $ø_{HT}$ and b.) 0.1 $ø_{HT}$. As can be seen, in the case that PVB is unpigmented, the filament width remains fairly consistent as the filament propagates over the substrate (arrows show direction of propagation of various filaments). In comparison, Figure 5b shows the case that the PVB contains 0.1 $ø_{HT}$. The image shows the presence of several filaments, one of which travels from the left of the image to the to right and appears to cross paths with a different filament which travels from the bottom of the image to the top. This observation is at odds with the behaviour of FFC as it occurs on iron, on which filaments never cross one another [29]. For example, Van Loo et al. found that if an active head strikes an active body the active filiform it is deflected at an angle approximately equal to the angle of incidence [29]. Ruggeri and Beck postulate that an active head does not cross the tail as it would then encounter a new source of oxygen meaning a change in the relative positions of the anodic and cathodic sites [5]. Slabaugh and Grotheer suggest that FFC heads are discouraged from progressing in areas of film from which the water soluble components have already been extracted [9].

The fact that corrosion filament crossing is observed on PVB coated ZAM implies that the differential aeration cell is less sensitive to any disruption caused when encountering a new source of oxygen. It was demonstrated previously that selective, HAc induced dissolution of Mg rich phases within the eutectic caused iron exposure [3]. As a result, a differential cathodic activation mechanism was proposed, in which anodic metal dissolution at the front of the filament is coupled to oxygen reduction at the back of the

filament head, electrocatalytically enhanced by a percolative route through the corroded ZAM layer to the underlying steel substrate [3]. However, subsequent precipitation of corrosion product in the tail region immediately behind the advancing may block these percolative networks to the underlying steel. The observation of an active filament advancing across the tail of another implies that 1.) sufficient Mg rich phases remain in the tail region of one filament to sustain adequate anodic activity at the leading edge of another to allow cross-filament propagation to continue and 2.) the principal cathodic site of the crossing filament located immediately behind anodic leading edge remains uninterrupted as it impinges on the tail of another. In addition, the filament crossing phenomenon also suggests that the porous corrosion deposit in the filament tail regions do not provide a sufficiently resistant barrier to further anodic dissolution of the underlying, previously corroded ZAM surface.

The ability of individual filaments to cross one another does not appear to affect the width of each filament and the width of the active head region appears to be similar prior to, and after, encounter with the tail of another filament. However, the width of each filament appears to decrease as the filament propagates further away from the defect. Figure 6 shows filament width as a function of filament propagation length for the case that FFC is initiated on 1.5Al-1.5Mg coated steel by injecting 2 µL of 1.5 mol.dm^{-3} HAc to a penetrative PVB coating scribe when PVB contains 0.1 $ø_{pig}$ Filament width is initially ~130-160 µm, but decreases to approximately half this value after travelling ~ 1.5 µm.

(Figure 5)

(Figure 6)

4. Discussion

The kinetics of FFC as it occur on ZAM is have been characterized in detail in previous publications [3]. The FFC corroded area increases linearly with time (Figure 3) for both the control and 0.05 $ø_{HT}$, this being consistent with a constant rate of FFC propagation and conservation of the head electrolyte [2, 4-5]. Another implication of linear kinetics is that the distance between the main cathodic site and leading anodic head remains constant [13]. In comparison, above 0.05 $ø_{HT}$, the growth of FFC corroded area tends to lower rates at longer holding times, as well as deviating from linearity.

In the absence of HT, filiform propagates at a substantially constant rate on ZAM, this finding being consistent with conservation of acetate electrolyte volume in the filiform head [2, 4-5]. In the case that the composition of the electrolyte contained within the head remains constant, its volume (which is in isopiestic equilibrium with the reference solution) is proportional to initiator HAc concentration. There does not appear to be a relationship between the width of each filament (diameter of head electrolyte) and rate of filament extension, this being consistent with mass transport control which may arise ohmically due to the transport of ions through poorly conducting media or along substrate/coating interfaces.

The deviation in linearity of FFC corroded area growth rate at longer holding times for $ø_{HT} > 0.05$ (Figure 3 inset) is consistent with a decrease in the rate growth in filament length (Figure 4) within phase 2 (broken trend lines). The rate at which the length of individual filaments increases appears to be highly dependent upon $ø_{HT}$ (Figure 4). The rate at which the filaments propagate decreases after an initial period (phase 1) at $ø_{HT} \geq 0.05$. The lower filament length growth rates observed after ~ 3 weeks (phase 2) for

correspond to tapering of filaments with lower filament head radius (width), or those for which width decreases as a function of length (Figure 5 and Figure 6). Such observations, namely the filament length growth rate being influenced by the filament width, is consistent with activation controlled FFC, where propagation is controlled by the underfilm cathode [13] and thinner filaments move more slowly than larger ones (in contrast to the ohmically controlled FFC observed on iron, for which filaments tend to travel at the same rate, regardless of width). A decrease in propagation rate as the filament becomes progressively more tapered is consistent with propagation under cathodic control and anodic ZAM dissolution being coupled with cathodic ORR on the exposed iron substrate towards the back of the droplet.

On samples containing 0.2 $ø_{HT}$, filament propagation has completely stopped after 4 weeks. The ability of HT to remove HAc from aqueous solution and displace carbonate as CO_2 has been demonstrated previously [39] and is related to the low pKa value (4.7) associated with HAc compared to carbonate and hydrogen carbonate anions [40]. It therefore seems plausible that HT acts to scavenge Ac^- via an anion exchange reaction (Equation 3), shown schematically in Figure 7. The formation of water via the acid base reaction (Equation 4) will result in an increase in head electrolyte volume. Excess H_2O acts to dilute the electrolyte present within the filament head, this reducing the number of aggressive anions per volume of electrolyte and resulting in an increased pH.

$$2HAc_{(aq)} + {CO_3^{2-}}_{(HT)} \rightarrow 2{Ac^-}_{(HT)} + {CO_3^{2-}}_{(aq)} \rightarrow \quad (3)$$

$$2HAc_{(aq)} + {CO_3^{2-}}_{(aq)} \rightarrow H_2O_{(l)} + CO_{2(g)} + 2{Ac^-}_{(aq)} \quad (4)$$

This neutralization process will be accompanied by evaporation, which takes place to maintain isopiestic equilibrium with the reference solution used. This loss in acetate will

reduce the volume of electrolyte present within the head electrolyte, and thus the filament width (diameter of electrolyte droplet).

(Figure 7)

It is possible to calculate the amount of coating HT required to replace all the Ac^- within the electrolyte. Table 4 shows the area of the 30 µm coating required to exchange Hac present within the head electrolyte in the case that ϕ_{HT} varies between 0.05 and 0.2. In all cases the coating volume per m^2 is assumed to be $3 \times 10^{-5} m^3$ and the head electrolyte is taken to be 2 µL aliquots of 1.5 $mol.dm^{-3}$ Hac ($3 \times 10^{-6} mols.\, m^{-2}$). It is clear from Table 4, that even at 0.2 ϕ_{HT}, a coating area of 3.6 cm^2 would be required to replace all of the Ac^- within the head. The small filament width, along with the highly concentrate nature of the head electrolyte, means that the filament would need to propagate a large distance before most of the Ac^- can be removed. However, the tapering of filaments observed in Figure 6 suggest that it is possible that the electrolyte concentration decreases to a point at which propagation may cease.

(Table 4)

5. Conclusions

In-coating HT leads to a reduction in the filiform total corroded area, average filament length, and average number of filiform corrosion filaments per defect observed on Zn-Al-Mg hot dip coated steel. The degree of inhibition scales with the level of HT added (with higher amounts of HT results leading to reduced corroded area and fewer, shorter filaments). HT is believed to scavenge Ac^- via an anion exchange reaction which results in an increase in head electrolyte volume and dilution of the head electrolyte. This neutralization process will be accompanied by evaporation and the loss in acetate will

reduce the volume of electrolyte present within the head electrolyte, and thus the filament width (diameter of electrolyte droplet). The finite amount of HT present in the coating limits the number of exchange reactions that occur and corrosion continues in the case of that the HT capacity is exhausted, as may occur at higher concentrations of Hac. HT is therefore believed to have potential as a viable, non toxic method of reducing the extent to which FFC is able to initiate and propagate on organically coated Zn-Al-Mg hot dip galvanized steel. This finding is significant given 1.) the lack of work pertaining to the inhibition of FFC occurring on ZAM, 2.) the increasing use of ZAM for industrial applications and 3.) the need to find non toxic replacements for inhibitors based on hexavalent chromium.

5. Acknowledgments

The authors would like to thank Tata Steel for providing samples and EPSRC for the funding for the Engineering Doctorate studentship via the Collaborate Training Account (GR/T11333/01).

The raw/processed data required to reproduce these findings cannot be shared at this time as the data also forms part of an ongoing stud

6. References

1. D. Thierry, D. Persson, G. Luckeneder, K. H. Stellnberger, Atmospheric corrosion of ZnAlMg coated steel during long term atmospheric weathering at different worldwide exposure sites, Corrosion Science. 148 (2019) 338-354. https://doi.org/10.1016/j.corsci.2018.12.033.
2. G.Williams, H. N.McMurray, Underfilm/coating corrosion, in: B. R. A. Cottis,M. Graham, R. Lindsay, S. Lyon, T. J. A. Richardson, D. J. D. Scantlebury, H. Stott, (Eds.), Shreir's Corrosion, Elsevier Science, 2009, pp. .988-2004.
3. N. Wint, D. Eaves, E. Michailidou, A. Bennett, J.R. Searle, G. Williams, H.N. McMurray, The kinetics and mechanism of filiform corrosion occurring on zinc-

aluminium-magnesium coated steel, Corrosion Science. 158 (2019) 108073. https://doi.org/10.1016/j.corsci.2019.06.028.

4. A. Bautista, Filiform corrosion in polymer-coated metals, Progress in Organic Coatings. 28 (1996) 49-58. https://doi.org/10.1016/0300-9440(95)00555-2.

5. R. T. Ruggeri and T. R. Beck, An Analysis of Mass Transfer in Filiform Corrosion, Corrosion-NACE. 39 (1983) 452-465. https://doi.org/10.5006/1.3581907.

6. G. Grundmeier, W. Schmidt, and M. Stratmann, Corrosion protection by organic coatings: electrochemical mechanism and novel methods of investigation, Electrochimica Acta. 45 (2000) 2515-2533. https://doi.org/10.1016/S0013-4686(00)00348-0.

7. G. Williams, H.N. McMurray, The mechanism of group (I) chloride initiated filiform corrosion on iron, Electrochemistry Communications. 5 (2003) 871-877. https://doi.org/10.1016/j.elecom.2003.08.008.

8. T. M.Watson, A. J. Coleman, G.Williams, and H. N. McMurray, The effect of oxygen partial pressure on the filiform corrosion of organic coated iron, Corrosion Science. 89 (2014) 46-58. https://doi.org/10.1016/j.corsci.2014.08.004.

9. W.H. Slabaugh, M. Grotheer, Mechanism of Filiform Corrosion, Industrial & Engineering Chemistry. 46 (1954) 1014-1016. https://doi/pdf/10.1021/ie50533a053.

10. W. Schmidt and M. Stratmann, Scanning kelvinprobe investigations of filiform corrosion on aluminum alloy 2024-t3, Corrosion Science. 40 (1998) 1441-1443. https://doi.org/10.1016/S0010-938X(98)00044-4.

11. J. H. W. de Wit, New knowledge on localized corrosion obtained from local measuring techniques, Electrochimica Acta. 46 (2001) 3641-3650. https://doi.org/10.1016/S0013-4686(01)00642-9.

12. N. LeBozec, D. Persson, D. Thierry, S.B. Axelsen, Effect of Climatic Parameters on Filiform Corrosion of Coated Aluminum Alloys, CORROSION. 60 (2004) 584-593. https://doi.org/10.5006/1.3287763.

13. G. Williams, H.N. McMurray, The Kinetics of Chloride-Induced Filiform Corrosion on Aluminum Alloy AA2024-T3, Journal of The Electrochemical Society. 150 (2003) B380-B388. https://doi:10.1149/1.1589020.

14. H.N. McMurray, G. Williams, S. O'Driscoll, Chromate Inhibition of Filiform Corrosion on Organic Coated AA2024-T3 Studied Using the Scanning Kelvin Probe, Journal of the Electrochemical Society. 151 (2004) B406-B414. https://doi.org/10.1149/1.1757460.

15. H.N. McMurray, A. Holder, G. Williams, G.M. Scamans, A.J. Coleman, The kinetics and mechanisms of filiform corrosion on aluminium alloy AA6111,

Electrochimica Acta. 55 (2010) 7843-7852. https://doi.org/10.1016/j.electacta.2010.04.035.

16. J.V. Kloet, W. Schmidt, A.W. Hassel, M. Stratmann, The role of chromate in filiform corrosion inhibition, Electrochimica Acta. 49 (2004) 1675-1685. https://doi.org/10.1016/S0013-4686(03)00256-1.

17. J.V. Kloet, W. Schmidt, A.W. Hassel, M. Stratmann, The role of chromate in filiform corrosion inhibition, Electrochimica Acta. 48 (2003) 1211-1222. https://doi.org/10.1016/S0013-4686(02)00829-0.

18. G. Williams, R. Grace, Chloride-induced filiform corrosion of organic-coated magnesium, Electrochimica Acta. 56 (2011) 1894-1903. https://doi.org/10.1016/j.electacta.2010.09.005.

19. C. Leygraf, J. Hedberg, P. Qiu, H. Gil, J. Henriquez, C.M. Johnson, W.R. Whitney Award Lecture: Molecular In Situ Studies of Atmospheric Corrosion, CORROSION. 63 (2007) 715-721. https://doi.org/10.5006/1.3278420.

20. C.M. Johnson, E. Tyrode, C. Leygraf, Atmospheric Corrosion of Zinc by Organic Constituents: I. The Role of the Zinc/Water and Water/Air Interfaces Studied by Infrared Reflection/Absorption Spectroscopy and Vibrational Sum Frequency Spectroscopy, Journal of The Electrochemical Society. 153 (2006) B113-B120. https://doi.org/10.1149/1.2164788.

21. C.M. Johnson, C. Leygraf, Atmospheric Corrosion of Zinc by Organic Constituents: II. Reaction Routes for Zinc-Acetate Formation, Journal of The Electrochemical Society. 153 (2006) B542-B546. https://doi.org/10.1149/1.2360740.

22. H. Gil, C. Leygraf, J. Tidblad, GILDES Model Simulations of the Atmospheric Corrosion of Zinc Induced by Low Concentrations of Carboxylic Acids, Journal of The Electrochemical Society. 159 (2012) C123-C128. https://doi.org/10.1149/2.072203jes.

23. P. Qiu, D. Persson, C. Leygraf, Initial Atmospheric Corrosion of Zinc Induced by Carboxylic Acids: A Quantitative In Situ Study, Journal of The Electrochemical Society. 156 (2009) C441-C447. https://doi.org/10.1149/1.3240878.

24. J. Hedberg, S. Baldelli, C. Leygraf, E. Tyrode, Molecular Structural Information of the Atmospheric Corrosion of Zinc Studied by Vibrational Spectroscopy Techniques: I. Experimental Approach, Journal of The Electrochemical Society. 157 (2010) C357-C362. https://doi.org/10.1149/1.3479207.

25. J. Hedberg, S. Baldelli, C. Leygraf, Molecular Structural Information of the Atmospheric Corrosion of Zinc Studied by Vibrational Spectroscopy Techniques: II. Two and Three-Dimensional Growth of Reaction Products Induced by Formic and Acetic Acid, Journal of The Electrochemical Society. 157 (2010) C363-C373. https://doi.org/10.1149/1.3479255.

26. D. Persson, C. Leygraf, Metal Carboxylate Formation during Indoor Atmospheric Corrosion of Cu, Zn, and Ni, Journal of The Electrochemical Society. 142 (1995) 1468-1477.https://doi.org/10.1149/1.2048598.

27. E. Johansson, C. Leygraf, B. Rendahl, Characterisation of corrosivity in indoor atmospheres with different metals and evaluation techniques, British Corrosion Journal. 33 (1998) 59-66. https://doi.org/10.1179/000705998798114769.

28. S. A. Katz, H. Salem, The toxicology of chromium with respect to its chemical speciation: a review. Journal of Applied Toxicology. 13 (1993) 217-224. https://doi.org/10.1002/jat.2550130314.

29. S. Langard, T. Norseth, Occurrence of lung cancer in workers producing chromium pigments, British Journal of Industrial Medicine. 40 (1983) 71-74 https://doi.org/ 10.1136/oem.40.1.71.

30. A. Sheffet, I. Thind, A. M. Miller, D. B. Louria, Cancer mortality in a pigment plant utilizing lead and zinc chromates, Archives of Environmental Health: An International Journal. 37 (1982) 44-52. https://doi.org /10.1080/00039896.1982.10667532.

31. A.Vaccari. Clays and catalysis: a promising future. 1999, Applied Clay Science, pp. 161- 198.

32. V.A.Drits, T.N.Sokolova, G.V.Sokolova, V.I.Cherkashin. Group, New Members of the Hydrotalcite-Manasseite. 1987. Clays and Clay materials, pp. 401-417.

33. S. Miyata. Anion-exchange properties of hydrotalcite like compounds. Clays and Clay Minerals, 1983. 31 (4): p.305-311.

34. M. Kendig and M. Hon. A hydrotalcite-like pigment containing an organic anion corrosion inhibitor. Electrochemical and Solid State Letters. 2005. 8(3) p. B10-B11.

35. H. N. McMurray and G. Williams. Inhibition of filiform corrosion on organic coated aluminium alloy by hydrotalcite-like anion-exchange pigments. Corrosion. 60 (2004), 219-228.

36. S. Miyata. Chem. Abst, 1980. 93.

37. W. T. Reichle. Anionic Clay Minerals. ChemTech. 16 (58) (1886). 58-63.

38. W. Holtmeier, G. Holtmann, W. F. Caspary, U. Weingärtner. On-demand treatment of acute heartburn with the antacid hydrotalcite compared with famotidine and placebo: randomized double-blind cross-over study. J Clin Gastroenterol. 41 (2007) 564-70.

39. B. M. Travália and M. B. Soares Forte, New Proposal in a Biorefinery Context: Recovery of Acetic and Formic Acids by Adsorption on Hydrotalcites. Journal of Chemical & Engineering Data. 65 (2020), 4503-4511.

40. A. Hayashi, N. Hara, K. Sugimura, H. Masuda, E. Oku, S. Fujikake, S. Noda, and H. Nakayama. Intercalation behavior of carboxylic acids and their sodium salts with layered double hydroxide in methanol. Clay Science. 20 (2016) 43-48.

41. S.Gh.R. Emad, X. Zhou, S. Morsch, S.B. Lyon, Y. Liu, D. Graham, S.R. Gibbon. How pigment volume concentration (PVC) and particle connectivity affect leaching of corrosion inhibitive species from coatings. Progress in Organic Coatings, 134 (2019) 360-372.

42. M.F. Montemor, Functional and smart coatings for corrosion protection: a review of recent advances, Surface and Coatings Technology. 258 (2014), 17-37.

43. S. P. V. Mahajanam and R. G.Buchheit. Characterization of inhibitor release from Zn-Al-[V10 O28]6- hydrotalcite pigments and corrosion protection from hydrotalcite-pigmented epoxy coatings. Corrosion, **64** (2008) 230–240.

44. M. L. Zheludkevich, S. K. Poznyak, L. M. Rodrigues, D. Raps, T. Hack, L. F. Dick, T. Nunes, M. G. S. Ferreira. Active protection coatings with layered double hydroxide nanocontainers of corrosion inhibitor. Corrosion Science. 52 (2010), 602–611.

45. M. Fedel, C. Zanella, L. Ferrari, F. Deflorian, Effect of the synthesis parameters of in situ grown Mg-Al LDHs on the filiform corrosion susceptibility of painted AA5005, Electrochimica Acta, 381 (2021).

46. H. D. Van Der Weijde, H. N. McMurray, T. Watson. 2006. Packaging for Packaging Food Products, Coated Substrates and Coating System for producing said packaging and and use of said packaging. WO2006/029842.

The raw/processed data required to reproduce these findings cannot be shared at this time as the data also forms part of an ongoing study.

7. Figure Legends

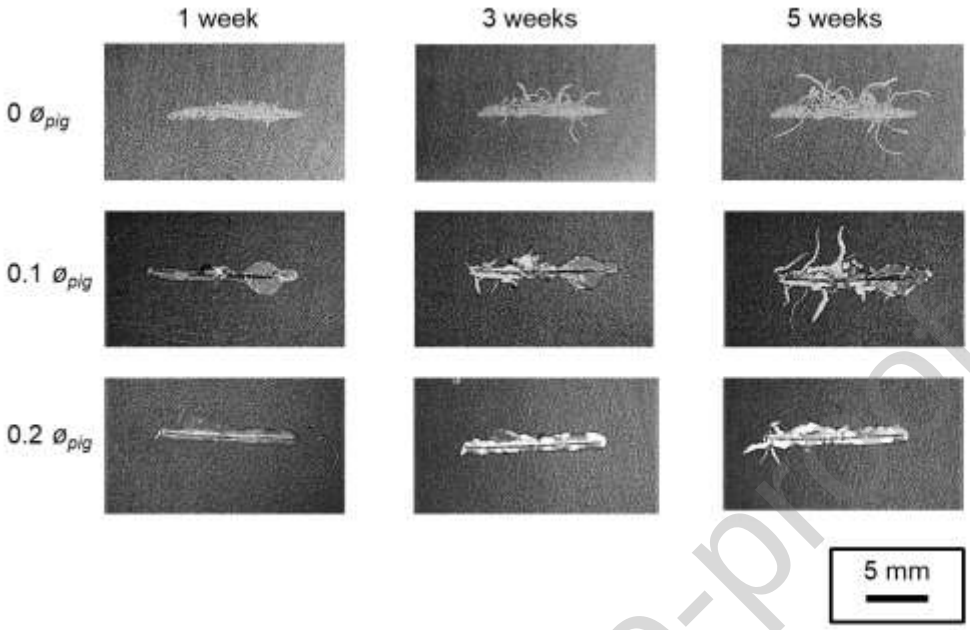

Figure 1. Optical images of FFC propagating on 1.5Al-1.5Mg coated steel 1 week, 3 weeks and 5 weeks after FFC has been initiated by injecting 2 µL of 1.5 mol.dm^{-3} HAc to a penetrative PVB coating scribe defect. Images are shown in the case that the PVB contains 0, 0.1 or 0.2 $ø_{pig}$ hydrotalcite.

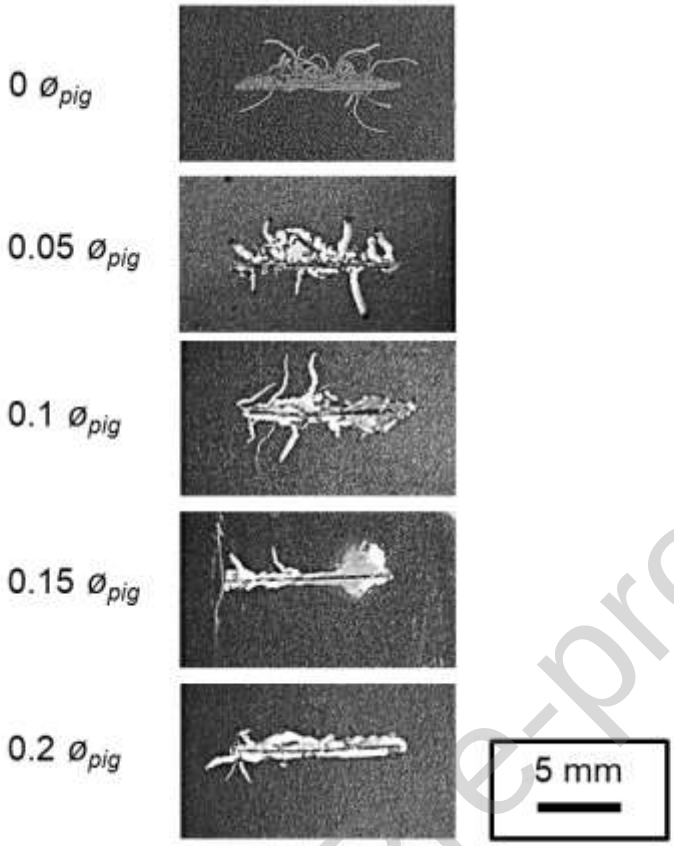

Figure 2. Optical images FFC on 1.5Al-1.5Mg coated steel 5 weeks after FFC has been initiated by injecting 2 µL of 1.5 mol.dm^{-3} HAc to a penetrative PVB coating scribe defect. Images are shown in the case that the PVB contains 0, 0.1 or 0.2 $ø_{pig}$ hydrotalcite.

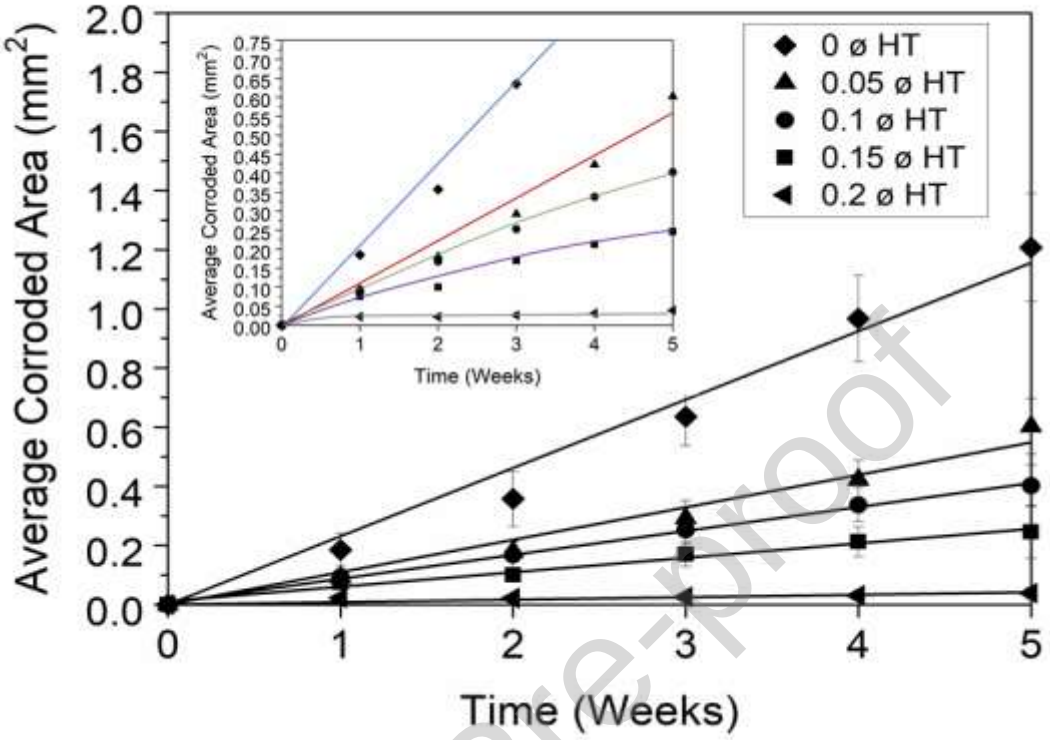

Figure 3. The time dependent corroded area for the case that FFC is initiated on 1.5Al-1.5Mg coated steel by injecting 2 µL of 1.5 mol.dm^{-3} HAc to a penetrative PVB coating scribe defect in the case that PVB contains varying amounts of hydrotalcite. The confidence limits (error bars) given correspond to ± one standard deviation on the mean of four measurements.

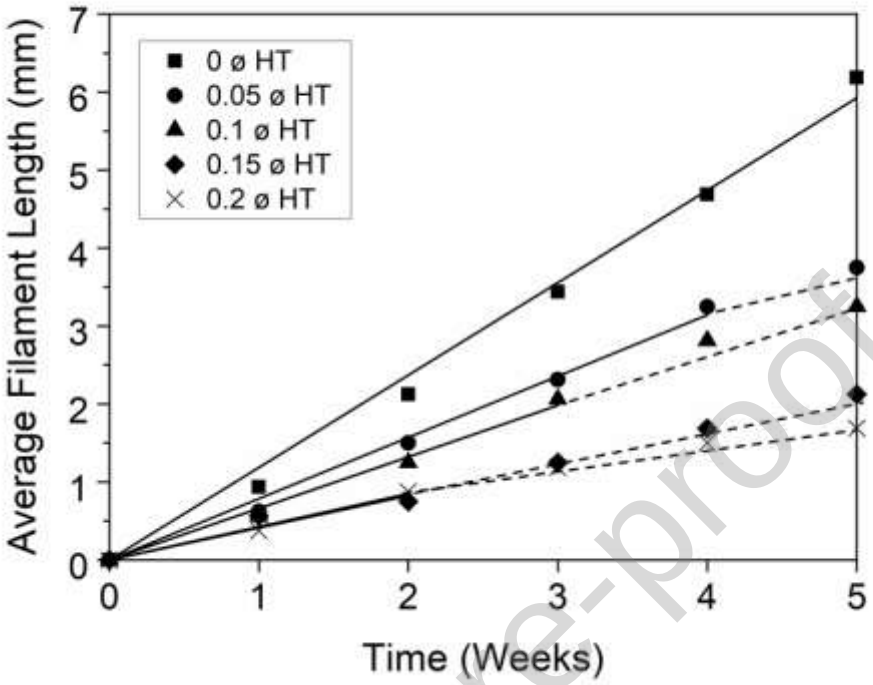

Figure 4. The time dependent filament length for the case that FFC is initiated on 1.5Al-1.5Mg coated steel by injecting 2 µL of 1.5 mol.dm^{-3} HAc to a penetrative PVB coating scribe defect in the case that PVB contains varying amounts of hydrotalcite. The confidence limits (error bars) given correspond to ± one standard deviation on the mean of four measurements.

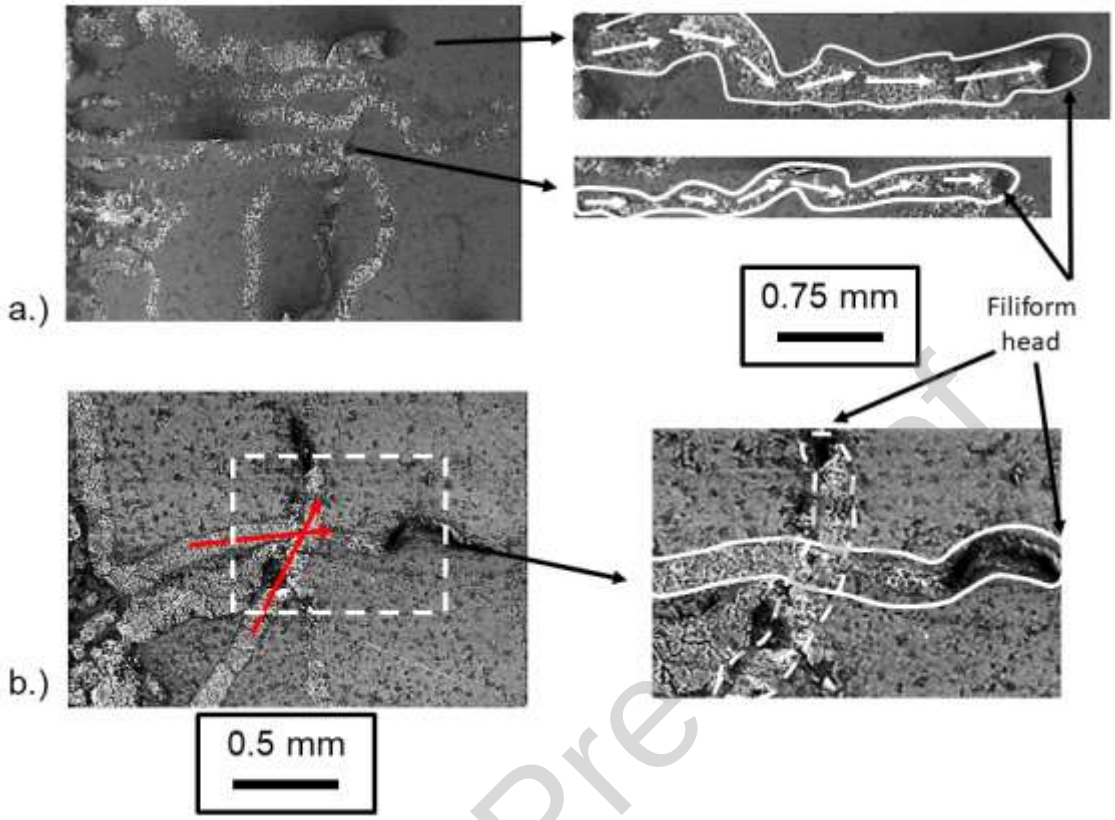

Figure 5. SEM images of filaments initiated on 1.5Al-1.5Mg coated steel by injecting 2 µL of 1.5 mol.dm^{-3} HAc to a penetrative PVB coating scribe in the case that the PVB contains a.) 0 $ø_{HT}$ and b.) 0.1 $ø_{HT}$

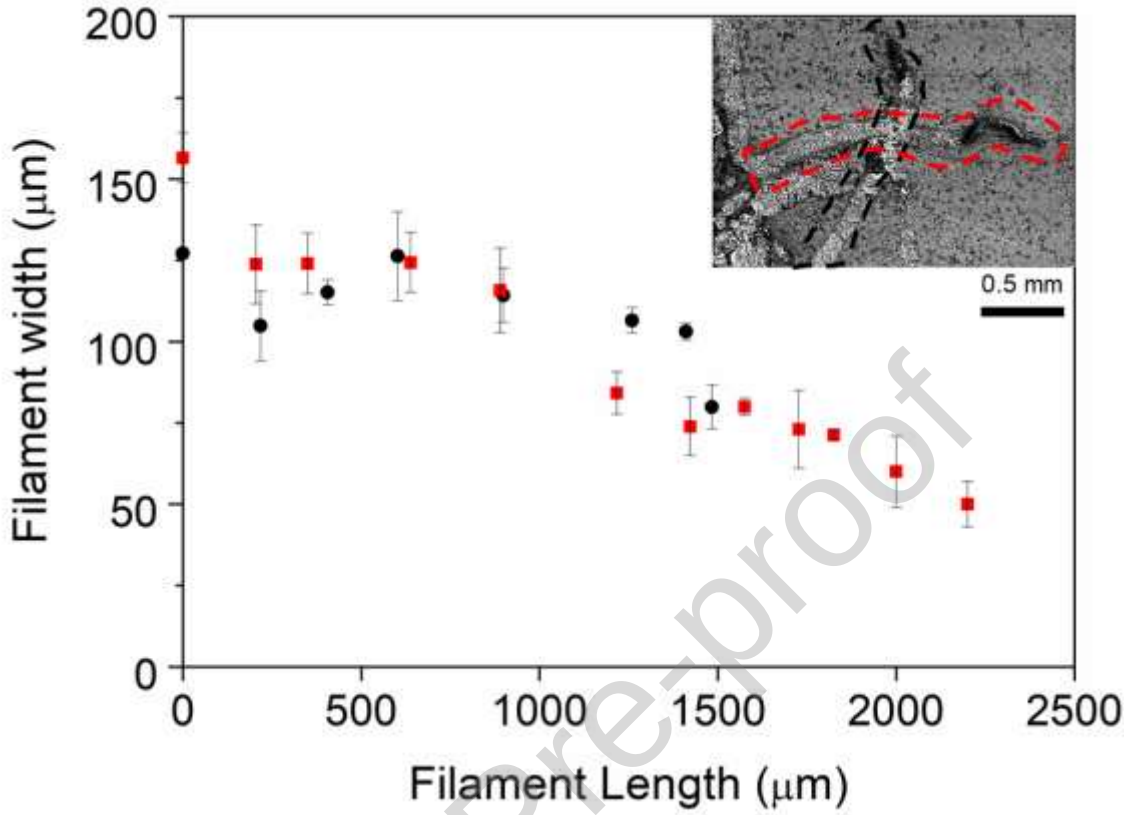

Figure 6. Plot of filament width as a function of length along propagating filament for the case that FFC is initiated on 1.5Al-1.5Mg coated steel by injecting 2 µL of 1.5 mol.dm^{-3} HAc to a penetrative PVB coating scribe when PVB contains 0.1 $ø_{pig}$

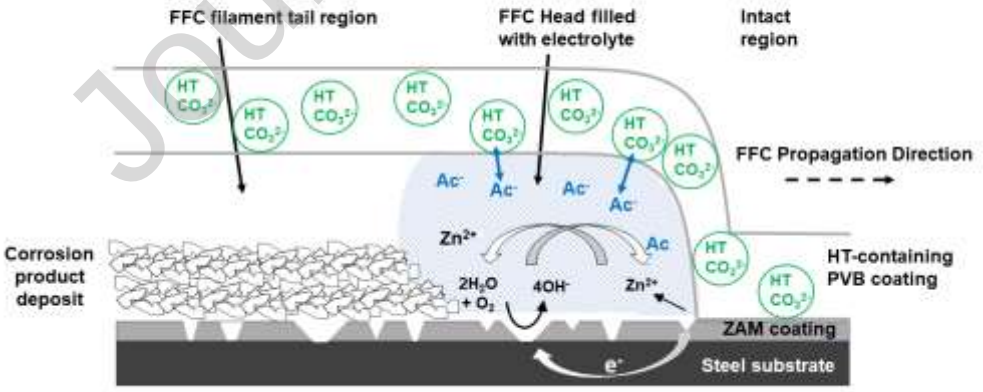

Figure 7. A schematic showing the anion exchange reaction during which in-coating HT is believed to scavenge Ac^- from the filiform head electrolyte, thus reducing the extent of filiform corrosion occurring on Zn 1.5Al-1.5Mg coated steel.

8. Tables

Table 1. Average number of filaments for the case that FFC is initiated on ZAM coated steel by injecting 2 µL of 1.5 mol.dm^{-3} HAc to a penetrative PVB coating scribe defect in the case that PVB contains varying amounts of hydrotalcite. The confidence limits (error bars) given correspond to ± one standard deviation on the mean of four measurements

$ø_{pig}$ Hydrotalcite	Number of filaments per Scribe
0	9±2
0.05	8±1
0.1	7±1
0.15	3±1
0.2	2±1

Table 2. Average FFC corroded area rate per 10 mm artificial scribe defect, for the case that FFC is initiated on ZAM coated steel by injecting 2 µL of 1.5 mol.dm^{-3} HAc to a penetrative PVB coating scribe defect in the case that PVB contains varying amounts of hydrotalcite

Time (weeks)	Corroded Area (mm^2)				
	0 $ø_{HT}$	*0.05 $ø_{HT}$*	*0.1 $ø_{HT}$*	*0.15 $ø_{HT}$*	*0.2 $ø_{HT}$*
0	0	0	0	0	0
1	0.19±0.05	0.09±0.03	0.09±0.02	0.08±0.01	0.02±0.01
2	0.36±0.09	0.18±0.03	0.17±0.05	0.10±0.01	0.02±0.01
3	0.64±0.10	0.29±0.06	0.25±0.05	0.17±0.04	0.03±0.01
4	0.97±0.15	0.42±0.07	0.34±0.05	0.21±0.05	0.03±0.02
5	1.21±0.18	0.60±0.09	0.40±0.07	0.25±0.09	0.04±0.02

Table 3. Average FFC corroded area rate and FFC length rate obtained when FFC is initiated on ZAM coated steel by injecting 2 µL of 1.5 mol.dm^{-3} HAc to a penetrative PVB coating scribe defect in the case that PVB contains varying amounts of hydrotalcite.

$ø_{HT}$.	**dA/dt** **mm^2.week^{-1}**	**dL/dt** **mm.week^{-1}** **Phase 1**	**dL/dt** **mm.week^{-1}** **Phase 2**
0	0.23±0.01	1.18±0.03	
0.05	0.11±0.01	0.79±0.02	0.50±0.01
0.1	0.08±0.01	0.66±0.02	0.59±0.09
0.15	0.05±0.01	0.41±0.05	0.46±0.01
0.2	0.01±0.01	0.43±0.02	0.28±0.02

Table 4. Calculations for the area of 30 µm PVB coating required to exchange 2 µL of 1.5 mol.dm^{-3} Hac head electrolyte in the case that $ø_{HT}$ varies between 0.05 and 0.2.

$ø_{HT}$	**0.05**	**0.1**	**0.15**	**0.2**
Volume of HT per m^2 $ø_{HT} \times$ Volume	15×10^{-7}	3×10^{-6}	4.5×10^{-6}	6×10^{-6}
Mass (g) of HT per m^2 ρ x V	3	6	9	12
Equivalents per m^2 Empirical (0.7 meq.g^{-1}) [37]	2.1 meq.m^{-2}	4.2 meq.m^{-2}	6.3 meq.m^{-2}	8.4 meq.m^{-2}
Area of coating (m^2) required to exchange 2 µL of 1.5 mol.dm^{-3} HAc	1.5×10^{-3}	7.1×10^{-4}	4.8×10^{-4}	3.6×10^{-4}

CRediT authorship contribution statement

N. Wint: Formal analysis, data curation, writing-original & draft, writing- review and editing, visualization.
D. Eaves: Validation, formal analysis, investigation, data curation.
G.Williams: Conceptualization, methodology, writing- review and editing, supervision
H.N. McMurray: Conceptualization, methodology, writing- review and editing, supervision

Declaration of interests

☒ The authors declare that they have no known competing financial interests or personal relationships that could have appeared to influence the work reported in this paper.

☐The authors declare the following financial interests/personal relationships which may be considered as potential competing interests:

Highlights

- In-coating carbonate exchanged hydrotalcite reduces filaments initiated on Zn-Al-Mg.
- Filiform corroded area decreases with increase in hydrotalcite volume fraction.
- Filament propagation rate decreases with increased hydrotalcite volume fraction.
- Decrease in filament width at reduced rates of filament propagation.
- Hydrotalcite thought to sequester anions or neutralise head electrolyte.